Remote Sens. **2015**, *7*, 8202-8223; doi:10.3390/rs70608202

OPEN ACCESS

remote sensing

ISSN 2072-4292

www.mdpi.com/journal/remotesensing

Article

Observing Land Subsidence and Revealing the Factors That Influence It Using a Multi-Sensor Approach in Yunlin County, Taiwan

Wei-Chen Hsu [1,2], Hung-Cheng Chang [2], Kuan-Tsung Chang [3], En-Kai Lin [2], Jin-King Liu [2] and Yuei-An Liou [4,*]

1 Department of Civil Engineering, National Chiao Tung University, No. 1001 University Road, Hsinchu 300, Taiwan; E-Mail: ianhsu@lidar.com.tw

2 LIDAR Technology Co., Ltd., 13F-3, No.32, Gaotie 2nd Rd., Zhubei City, Hsinchu 302, Taiwan; E-Mails: harrychang@lidar.com.tw (H.-C.C.); easyko23@lidar.com.tw (E.-K.L.); jkliu@lidar.com.tw (J.-K.L.)

3 Department of Civil Engineering and Environmental Informatics, Ming Hsin University of Science and Technology, No.1, Xinxing Rd., Xinfeng, Hsinchu 304, Taiwan; E-Mail: ktchang@must.edu.tw

4 Center for Space and Remote Sensing Research, National Central University, No.300, Jhongda Rd., Jhongli, Taoyuan 320, Taiwan

* Author to whom correspondence should be addressed; E-Mail: yueian@csrsr.ncu.edu.tw; Tel.: +886-3-422-7151 (ext. 57631); Fax: +886-3-425-4908.

Academic Editors: Richard Gloaguen, Ioannis Gitas, Dale A. Quattrochi and Prasad S. Thenkabail

Received: 12 October 2014 / Accepted: 8 June 2015 / Published: 19 June 2015

Abstract: Land subsidence is a worldwide problem that is typically caused by human activities, primarily the removal of groundwater. In Western Taiwan, groundwater has been pumped for industrial, residential, agricultural, and aquacultural uses for over 40 years. In this study, a multisensor monitoring system comprising GPS stations, leveling surveys, monitoring wells, and Persistent Scatterer Interferometric Synthetic Aperture Radar (PS-InSAR) was employed to monitor land subsidence in Western Taiwan. The results indicate that land subsidence in Yunlin County was mainly affected by the compaction of subsurface soils and over-pumping of groundwater from deep soils. The study area comprised western foothills, characterized by sediments containing predominantly gravel, and coastal areas, where clay was predominant. The subsidence in coastal areas was more severe than that in the western foothills, as a result of groundwater removal. An additional factor affecting subsidence was the compaction of deep layers caused by deep groundwater

removal and the deep-layer compaction was difficult to recover. Based on multisensor monitoring results, severe subsidence is mainly affected by compaction of subsurface soils, over-pumping of groundwater from deep soils, and deep soil compaction.

Keywords: land subsidence; groundwater; leveling; Global Positioning System (GPS); monitoring well; PS-InSAR

1. Introduction

Groundwater is an essential natural and national resource because it provides drinking water for urban and rural communities, supports irrigation and industry, sustains the flow of streams and rivers, and maintains riparian and wetland ecosystems. Land subsidence is the settling or sinking of the surface of the earth caused by downward movement of subsurface earth materials. Land subsidence is typically caused by human activities. It has become a global problem and is primarily caused by the removal of groundwater [1–4]. Subsidence can cause numerous problems, including changes in elevation that damage structures such as storm drains, sanitary sewers, roads, railroads, levees, bridges, and public and private buildings. Furthermore, subsidence increases the potential for flooding [5]. The need to monitor and mitigate land subsidence is clearly urgent [6–9].

Land subsidence occurs in municipalities and counties throughout Taiwan, including Taipei and Yilan in the north, and Changhua, Yunlin, Chiayi, and Pingdong in Central and Southern Taiwan [10,11] as shown in Figure 1. Maximal subsidence ranges from 1.2 m to 3.2 m, affecting an area of 2000 km^2. The most severely affected areas are located in Yunlin County. Their effects include dike failures, seawater encroachment in coastal aquifers, coastal inundation, and salinity intrusion. Recent national construction projects, such as a high-speed railway, expressways, urban rapid transportation systems, and science-based industrial parks have been adversely influenced by land subsidence, jeopardizing public safety.

In light of the negative impacts of land subsidence on the environment, Taiwan's government has constantly supported mass projects in recent two decades or so to monitor land subsidence and to understand its causes and the factors that influence it, which are then considered in order to initiate and enforce policy to prevent further land subsidence and, if possible, even attempt subsidence recovery. Among the many project results, Hung *et al.* [6] used multiple equipment to monitor land subsidence, including leveling, multi-level compaction monitoring wells, continuous GPS, and differential radar interferometry. They gave a general description of land subsidence monitoring sensors, including leveling, with a primary focus on quantifying subsidence and conducting an inter-comparison analysis on the measurements.

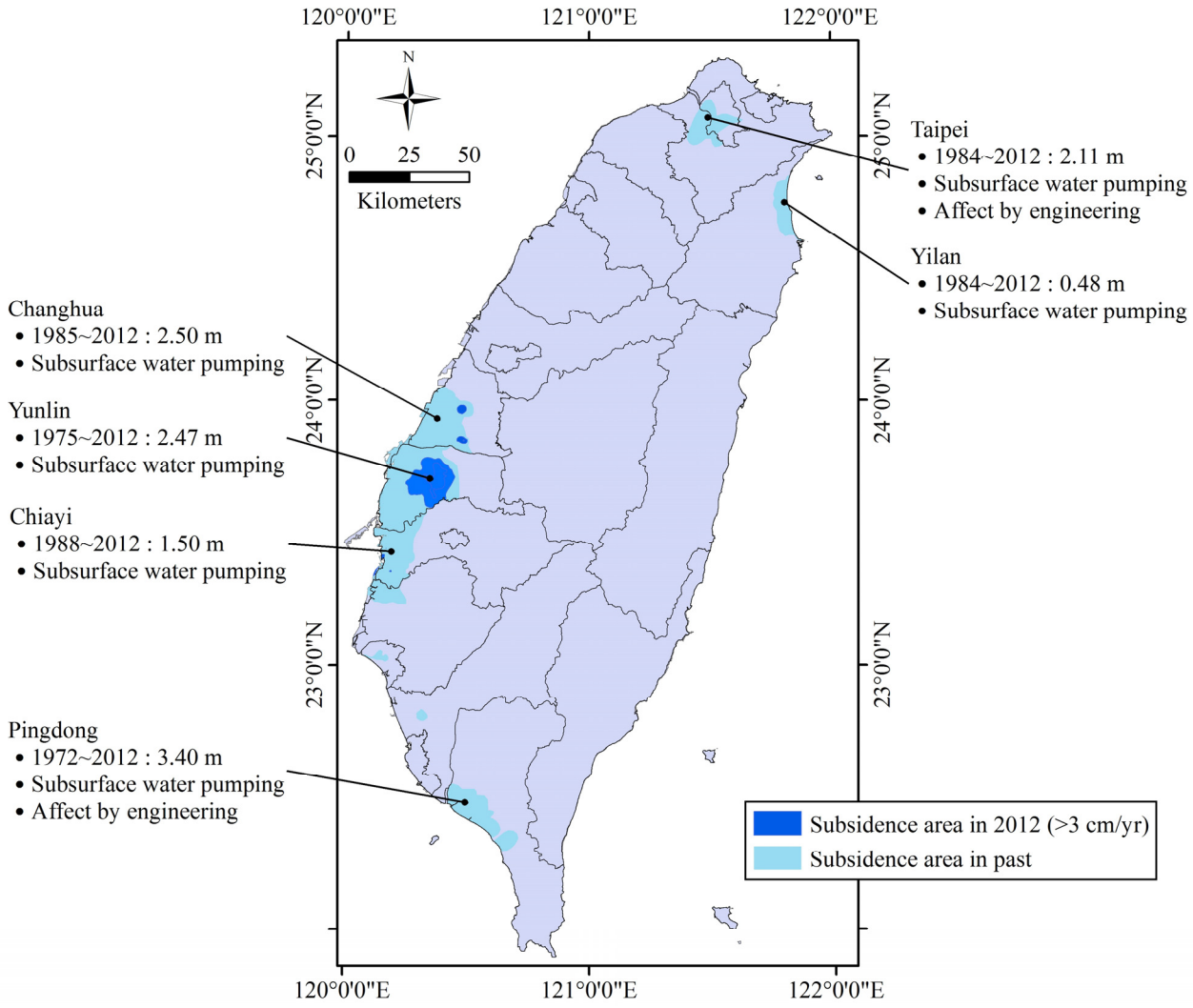

Figure 1. Distribution of land subsidence in Taiwan from 1972 to 2012 (adapted from the Water Resources Agency, Ministry of Economic Affairs, Taiwan).

In this study, it is our intention to improve understanding of the relevant land subsidence issues beyond Hung *et al.* [6] in two respects. First, we update the status of the land subsidence monitoring campaigns in the study region until the end of 2013 by using a comprehensive monitoring system that consists of various sensing equipment and techniques, including traditional leveling surveys, continuous GPS stations, monitoring wells, and PS-InSAR, according to the guidelines of groundwater conservation management and land subsidence mitigation plans. Secondly and most importantly, the possible main factors affecting land subsidence and its distribution are revealed. This is very crucial information to assist the government in setting up rules to take precautions and tackle the resulting environmental problems, in order to bring the greatest benefit to the people.

2. Study Area

The study area is characterized by severe land subsidence and is located in Yunlin County, south of the Jhuoshuei River alluvial fan. The Jhuoshuei River alluvial fan constitutes the largest aquifer in Taiwan and extends from the Wu River in the north to the Beigang River in the south and from the Baguashan Tableland and Douliou Hill in the east to the Taiwan Strait in the west, as shown in Figure 2.

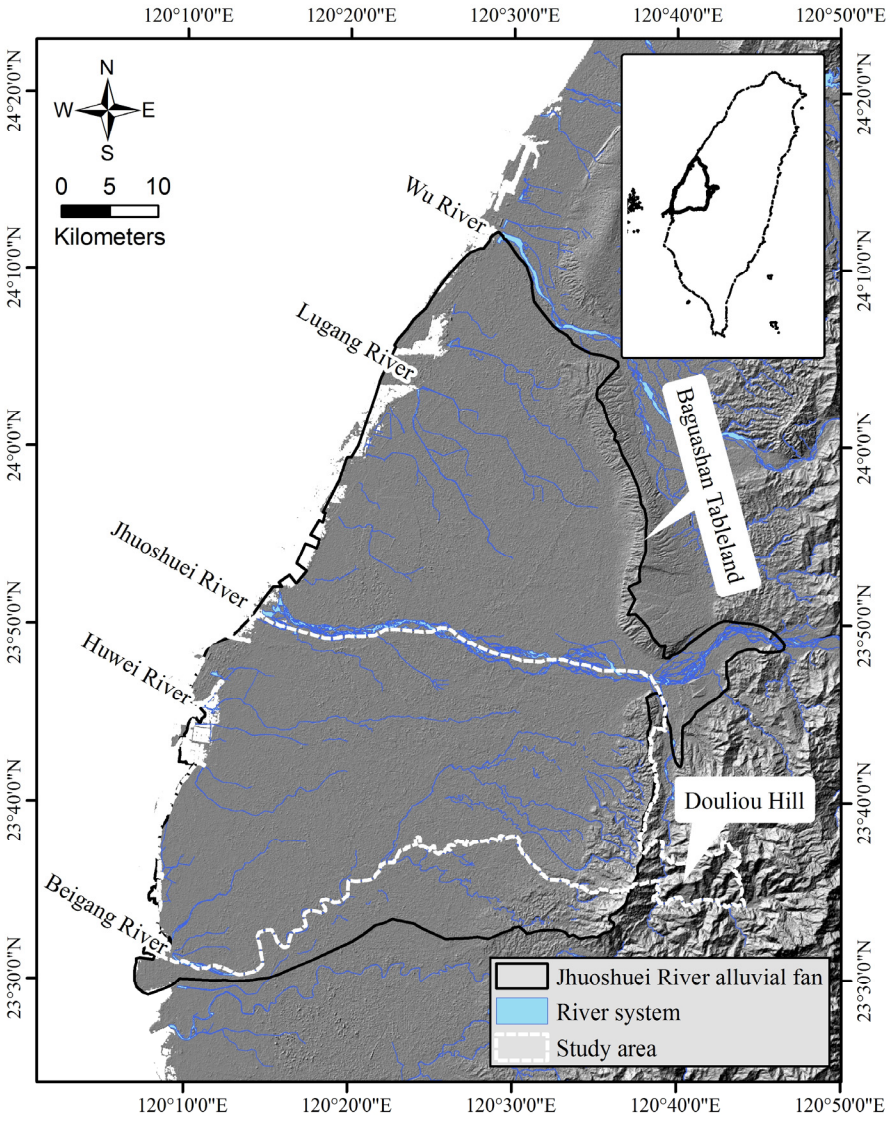

Figure 2. The white dash line indicates the study area south of the Jhuoshuei River alluvial fan.

The Jhuoshuei River alluvial fan is composed of unconsolidated sediments, mainly gravel, sand, and mud, which are transported by the Jhuoshuei, Lugang, and Huwei Rivers from the Pleistocene Toukoshan Formation in the east part of the alluvial fan. The sediment deposits in the Jhuoshuei River alluvial fan are the result of frequent flooding that has led to the formation of large-grain-size material, including gravel and coarse-grained sand, constituting an overlapping, layered distribution [12].

During marine transgression, mud covers an aquifer, thus forming an aquitard. In the Jhuoshuei River alluvial fan, marine transgression and regression have formed four aquifers and four aquitards that exhibit interlocking sedimentary layers, and also cause the thickness to decrease toward the inland for the aquitards, and toward the coast for the aquifers. Four aquifers merge at the top of the alluvial fan. Figure 3 depicts a hydrogeological model of the Jhuoshuei River alluvial fan and clearly shows that the aquifers and aquitards are formed by marine transgression and regression [12].

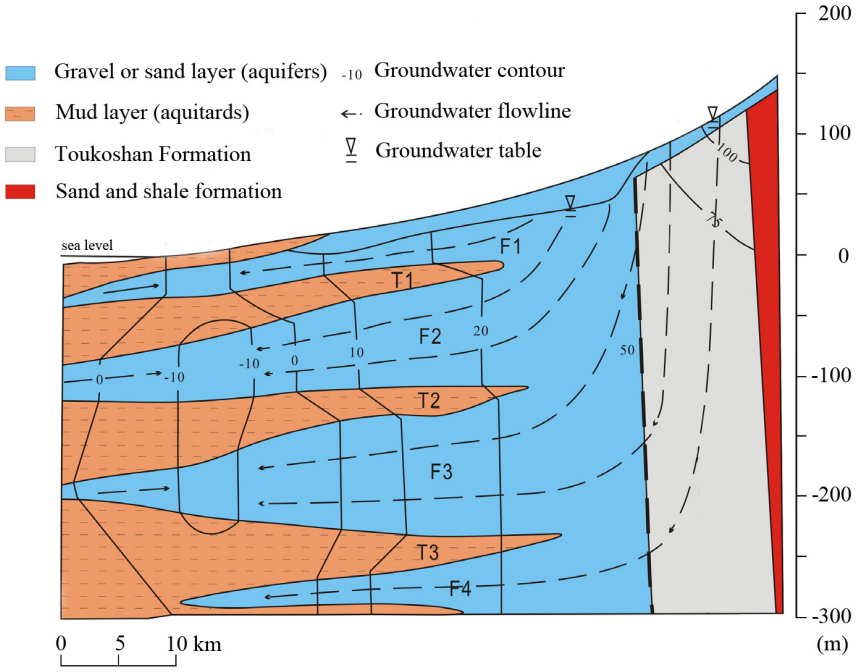

Figure 3. The east-west hydrogeology concept model of the Jhuoshuei River alluvial fan, composed of four aquifers and aquitards (adapted from [12]).

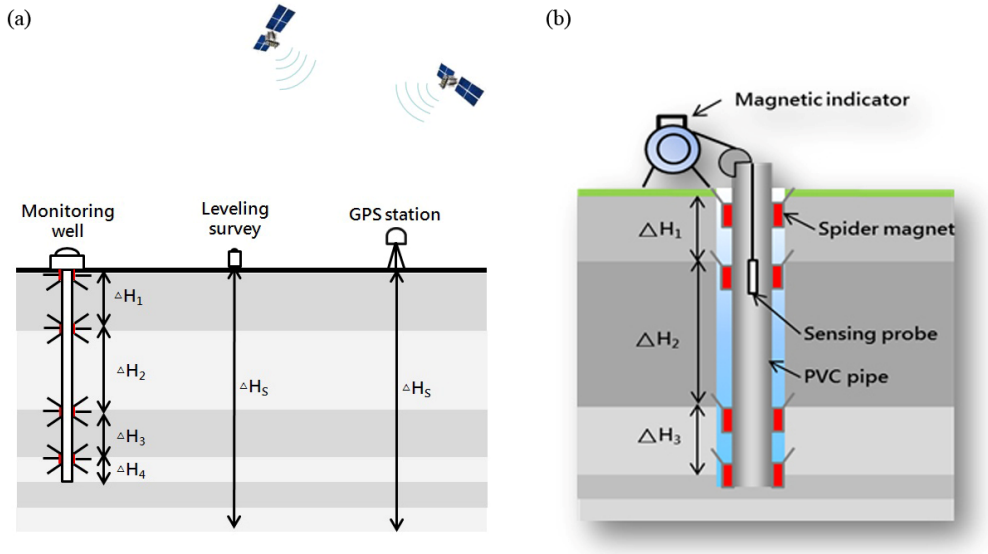

Figure 4. (**a**) Integrated multisensor system for monitoring land subsidence; (**b**) principle of monitoring wells for observing land subsidence.

3. Methodologies

In this study, the leveling surveys, permanent GPS stations, monitoring wells, and PS-InSAR were integrated into a multisensor monitoring system to monitor the land subsidence in Yunlin County as shown in Figure 4. The survey period was in 2012. In addition, this study collected the leveling data from 1992 to 2011, permanent GPS data from 2001 to 2011, monitoring well data from 1996 to 2011, and SAR images from 2007 to 2010, which were surveyed by the Industrial Technology Research

Institute to analyze land subsidence characteristics. Table 1 shows the sampling strategies used to ensure spatial and temporal resolution and accuracy. The survey methods are described as follows.

Table 1. Sampling strategies for ensuring spatial and temporal resolution and accuracy with the multisensor subsidence monitoring system.

Methods	Dense Array */ Spatial Resolution **	Survey Frequency/Period	Survey Period	Vertical Accuracy	Usage
Leveling survey	1.5–2 km *	1 year/1992–2012	1 year	<1 cm	For subsidence rate of each individual benchmark and isopleth of annual subsidence rate for 3 cm
Continuous GPS stations	5–20 km *	1 week/2001–2012	1 week	<1 cm	For a comparison with the other two observations to understand subsiding mechanism
Monitoring wells	5–15 km *	1 month/1996–2011	1 month	<0.5 cm	For a comparison with the other two observations to understand mechanism
PS-InSAR (ALOS)	25 m **	46 days/2007–2010	46 days	<1 cm	Feasibility study by comparing with those historical results

3.1. Leveling Survey

The leveling survey method involved the use of a Trimble DINI digital level with LD12 bar code rods to determine the benchmark networks from 2012 to 2013 with calibration implemented by National Measurement Laboratory R.O.C before surveying is conducted. The requirements for the leveling measurements followed the standards of the TWVD2001 first-order and class II leveling enforced by the Department of Land Administration, Ministry of Interior, Taiwan. Observations were made by comparing an observed height with a reference benchmark that was assumed to be fixed and with known ground deformation. For comparison with the previous leveling results, most locations of benchmarks are consistent with the past layout. However, leveling survey networks have been reorganized. There was a total of 383 benchmarks in the investigation area of Yunlin County, the total length of the leveling network is 502 km, and the distance between benchmarks is around 1.5–2.0 km (Figure 5). This study adopted 102 routes forming 26 loops and used BFFB survey method to measure the height of the benchmarks related to the LJ9029 located in the western foothills, which is a relative stable area (Figure 5).

To examine the stability of the reference point LJ9029, two test methods were performed: (1) the leveling procedure was adopted to determine the elevation of LJ9029 with respect to nearby known first-order benchmarks; and (2) a static GPS survey was conducted to verify the horizontal displacements of the LJ9029 and its neighboring known first-order benchmarks. The stability results indicate that absolute change of elevation difference between LJ9029 and nine first-order benchmarks range from 0.0 to 4.2 mm. In addition, the maximum horizontal displacement of neighboring benchmarks is 2.6 cm, so it is believed LJ9029 is located on a stable region. In order to maintain a high-precision leveling survey, the required accuracy for the final adjustment of the leveling survey is 3 mm$\sqrt{K}$, where K is the length of a surveying segment in kilometers. Leveling survey data were adopted to monitor annual land-surface deformation and used to generate the subsidence isopleth map. In the data processing, the errors with

collimation and earth's curvature were corrected, while the atmospheric refraction is not corrected without a known or measured atmospheric profile from collocated sounding equipment. A least squares method was utilized to adjust the data.

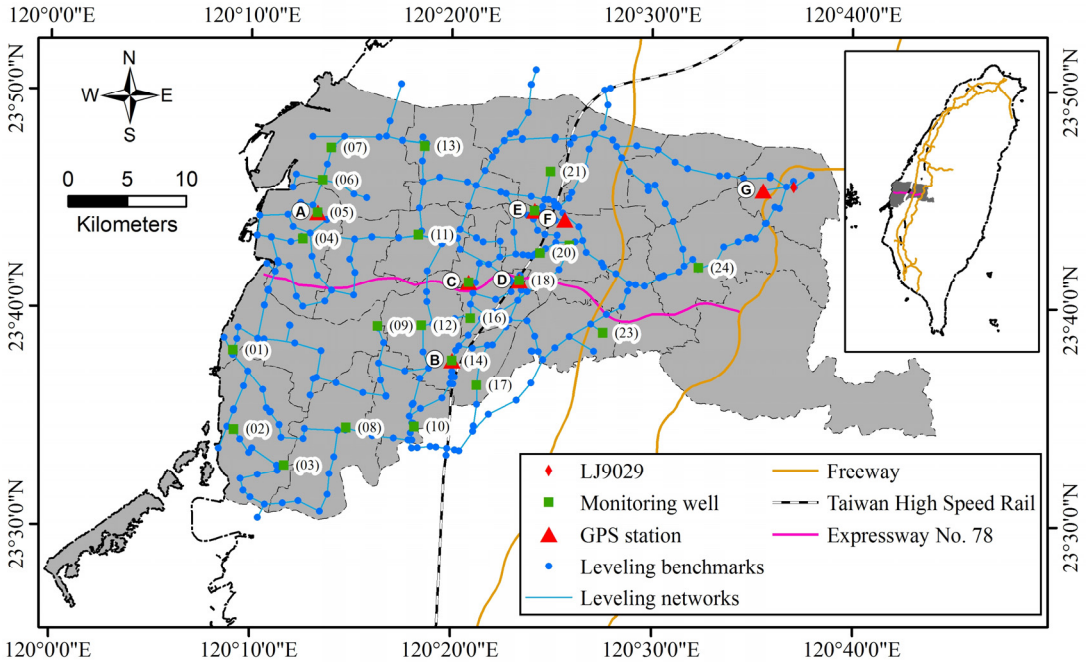

Figure 5. Leveling survey networks, benchmarks, GPS stations, and monitoring wells for land subsidence measurement in the study area. Monitoring wells are denoted (1)–(24) and GPS stations are denoted Ⓐ–Ⓖ.

3.2. Permanent GPS Survey

Seven continuous GPS monitoring stations in Yunlin County were used in this study to monitor land-surface deformation from 2012 to 2013 (Figure 5). These stations were installed on the same pillars located in areas undergoing substantial subsidence to provide regular and frequent observations. Monitoring signals and observation data were transmitted to a remote server through the Internet. Like most GPS survey practices, the epoch interval was 30 seconds with 15-degree elevation cutoff. The Bernese 5.0 [13] was used to calculate the weekly movement of GPS stations relative to an IGS station called TWTF. TWTF is located in Taoyuan city in Taiwan over the Eurasia plate with ITRF coordinates (X, Y, Z) = (−2,994,425.04, 4,951,312.24, 2,674,498.60), in meters, and Latitude = +245,712.96; Longitude = +1,210,952.20; and elevation = 203.122 m. Its receiver type is ASHTECH Z-XII3T with firmware version Z-XII3. It was installed on 1 August 2001. Its antenna type is ASH701945C_M SCIS with a 30 m Andraw FSJ1-50A cable. In order to understand atmospheric influence on GPS surveying and to even reduce the atmospheric effect [14,15], the site is also equipped with meteorological instrument MET-3 A, manufactured by Paroscientific, Inc., with a high sampling rate of 5 s, and high accuracies of 2%, 0.08 hPa, and 0.5 degrees for relative humidity, pressure, and temperature, respectively.

3.3. Monitoring Wells

In this study, 24 monitoring wells were used (Figure 5). Figure 4b shows the components of the monitoring wells. Magnetic rings were installed at the boundaries of sedimentary layers to enable distinguishing gravel, sand, silt, and clay. The locations of the magnetic rings of each well were measured monthly to observe the relative compaction of the sedimentary layers from 2012 to 2013. This information was critical in elucidating the relationship between the water extraction and subsidence mechanisms.

3.4. PS-InSAR

In order to accurately measure the ground displacement, the PS-InSAR technique, a more accurate and improved analysis algorithm as compared to other InSAR methods, was also adopted in our research. In total, twenty images were obtained from the phased array-type L-band SAR for the current study. Out of the twenty images, fourteen images were selected to form paired images in order to determine the land subsidence for further comparison with that measured by the leveling results. The acquisition time of the ALOS PALSAR images selected from the archives was between 15 February 2007 and 26 December 2010 (Table 2). Figure 6 depicts a SAR intensity image of the study area (33 km × 54 km), including the townships of Sihu, Erhlin, and Sicho in Changhua County to the north and the townships of Huwei, Tuku, and Yuenchang in Yunlin County to the south. The Hydro-Yun #88 benchmark was used as a reference point because the site is stable and has exhibited no detectable deformation over the past few years.

Table 2. SAR image pairs used in this study.

Image	Date	Perpendicular Baseline (m)	Temporal Baseline (Days)
1	2007/02/15	330.3	−966
2	2007/08/18	657.9	−782
3	2007/10/03	333.8	−736
4	2008//01/03	580.6	−644
5	2008/07/05	721.8	−460
6	2009/01/05	1223.9	−276
7	2009/08/23	240.6	−46
8 *	2009/10/08	/	/
9	2010/01/08	90.1	92
10	2010/02/23	641.1	138
11	2010/07/11	964.5	276
12	2010/08/26	1262.4	322
13	2010/10/11	1254.6	368
14	2010/11/26	1206.1	414

*: Image no. 8 is the PS-InSAR master image; the others are slave images.

Doris Software for Interferometric SAR processing from Delft University of Technology was used to perform the D-InSAR processing. Subsequently, the method by Mora et al. [16], and the Matlab program by Yang et al. [17] were used for PS-InSAR processing. The PS-InSAR data processing is briefly described here: (1) subset the study area from the image dataset; (2) compute the baselines of every pair;

(3) select a pair that exhibits a minimal temporal baseline to generate an interferogram of the topographic effects; (4) select a minimal temporal baseline as master image and set all other images as slave images, and then select the image pairs for further processing; (5) generate deformation interferograms and corresponding coherence maps for all paired images; (6) generate topographic interferograms for all paired images; (7) compute the difference between deformation and topographic interferograms for all paired images, (8) select the permanent scatterer candidate (PSC) points based on the coherence maps. A PSC point is selected when the coherence of all identical pairs is larger than the threshold; (9) compute PS-InSAR by using the phase information of each PSC, extracting permanent scatterer (PS) points and their range deformation; and (10) convert the slant range deformation to vertical deformation at the target of interest by multiplying the line-of-sight (LOS) deformation by the cosine of the incident angle.

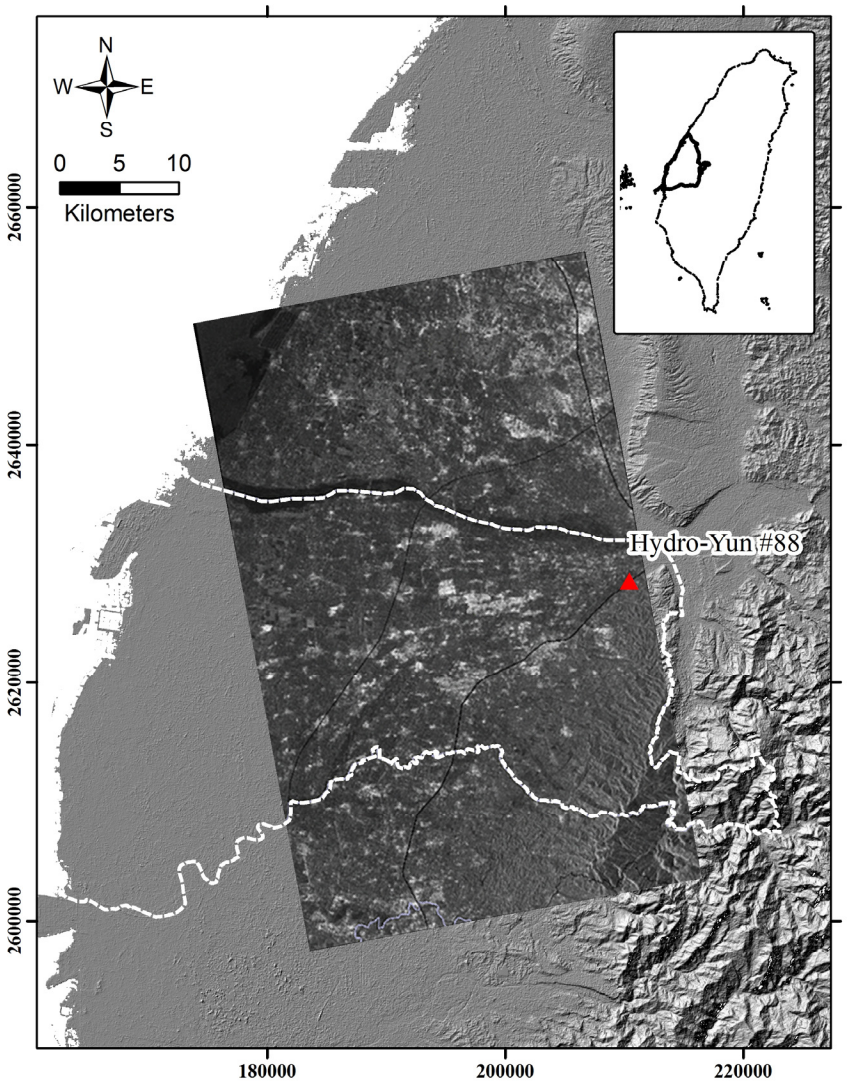

Figure 6. SAR intensity image of the study area (white dash line).

In data processing, generally a coherence threshold value of 0.4 or higher is chosen, as a higher threshold is better. In this study, a value of 0.34 for the threshold was selected in order to preserve a sufficient number of PSC points for extracting PS points as suggested by Yang [18] based on the previous experiences of PS-InSAR processing in the area of concern. The mean, minimum, and maximum coherences of PS are 0.63, 0.44, and 0.88, respectively. Finally, PS-InSAR was performed using the

phase information on each PSC and extracted 9413 PS points with range results for further comparison with leveling results.

Note that the displacement information revealed by PS-InSAR is along the LOS direction. For our investigation, the incident angle of image center is 38.7° for the RADAR data. According to characteristics of ALOS radar images with swath width of 70 km and track altitude of 691.65 km, as compared to earth diameter of 6371 km, the incident angles for the two edges of the image are 36.5° and 40.8°, respectively. Due to the fact that the annual horizontal movements for the two edges are smaller than 1 mm/y, the incident angle for all the areas of concern can be considered a constant 38.7°. That is, the incident angles of the radar beam in the near and far range are assumed to be fixed. Furthermore, based on the permanent GPS horizontal velocity analysis, Hung [19] found that the horizontal displacement in the study area was close to zero. Therefore, we did not consider the horizontal motion of PS-InSAR in this study.

4. Results

4.1. Leveling Survey

For over 40 years, in the western alluvial plains of Taiwan, groundwater has been extracted for industrial, residential, and agricultural uses. However, since 1980, the carrying capacity of certain plain lands in this region has been severely exhausted because of rapid economic and population growth. From 1980 to 1990, the extraction of groundwater used in aquacultural development along the coastal areas has caused severe land subsidence in the region. Since 1996, the subsidence center has migrated inland.

From 2012 to 2013, the leveling survey corrects the collimation and Earth's curvature. A least squares adjustment method was utilized to adjust the data. The average root mean square error per kilometer for leveling routes is ±0.62 mm$\sqrt{K}$. Loop misclosure errors range from 0.01 to 7.97 mm, which fulfill the required accuracy of 3 mm$\sqrt{K}$ with tolerances of 2.53 mm. Elevation of the reference benchmark LJ9029 is fixed as 84.58912 m in the adjustment computation of overall leveling networks. The number of observations is 410. The degree of freedom is 26. The weighting is by the inverse distance of level routes. The adjustment result shows that posterior root mean square error per kilometer for level routes is±0.493 mm$\sqrt{K}$ with mean error 6.4 mm and maximum standard deviation 8.65 mm. Finally the adjusted elevation for each benchmark can be used to calculate a subsidence isopleth map by the Kriging interpolation method.

Figure 7 shows the cumulative subsidence calculated in the leveling survey. The maximal land cumulative subsidence was –50 cm from 1992 to 1999 (Figure 7a) and increased to −150 cm from 1992 to 2013 (Figure 7g). In the past 14 years, the cumulative subsidence has increased by −100 cm. The three main subsidence areas were located in the Mailiao (cumulative subsidence near −100 cm), Taixi (cumulative subsidence near −80 cm), and Yuanzhang-Tuku-Baozhomg (cumulative subsidence near −150 cm; Figure 7g). Most subsidence occurred in the western part, and slight subsidence appeared in the eastern part with a boundary (black dash line in Figure 7) between them, almost located along a −20 cm to −50 cm contour line over the past 14 years. According to the leveling survey results, the subsidence phenomena were divided into three parts: severe subsidence in the center of the study area, moderate subsidence in the coastal area, and slight subsidence in the western foothills.

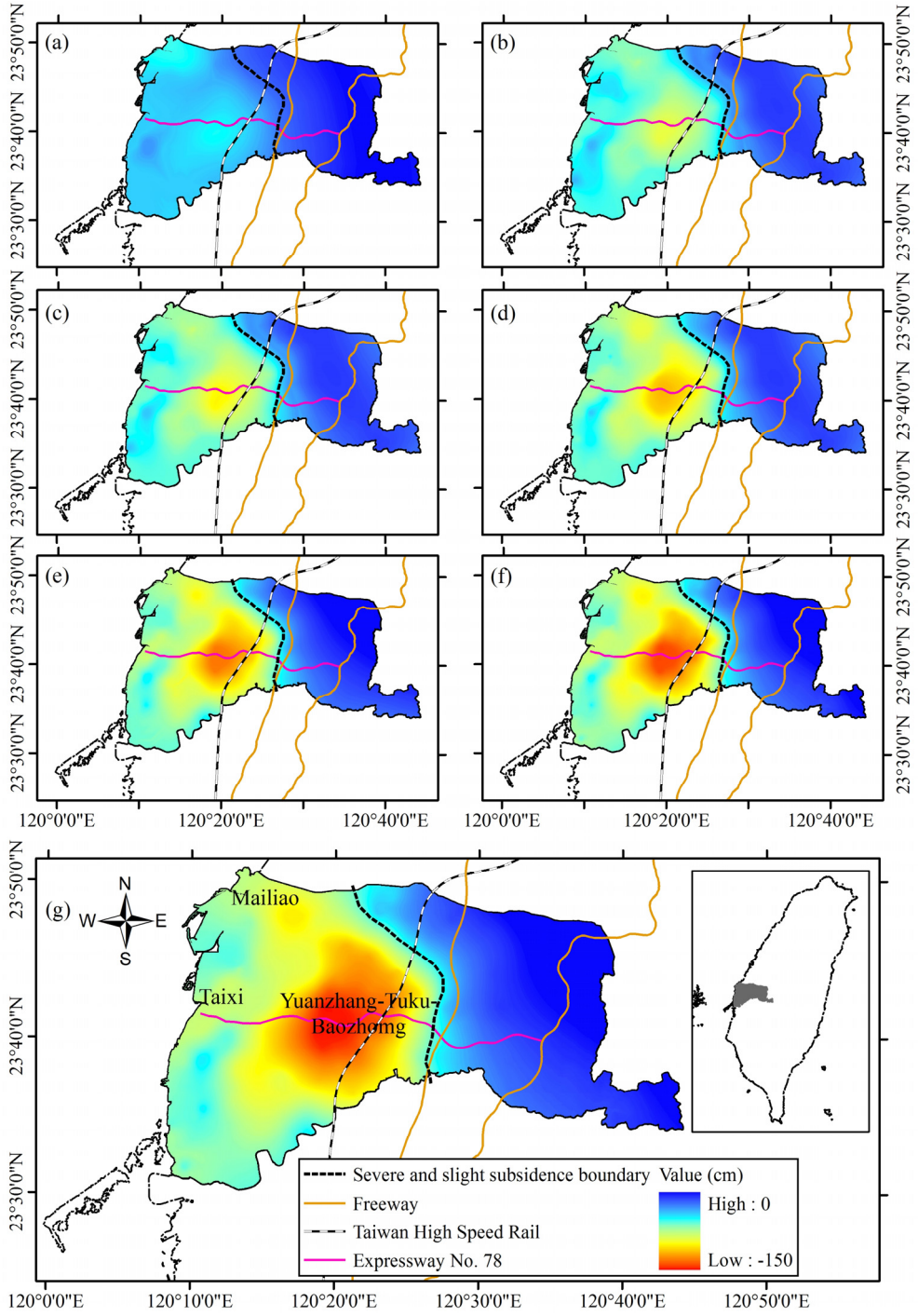

Figure 7. Cumulative land subsidence obtained by leveling data in Yunlin County from 1992 to 2013. The figure shows various time spans of cumulative land subsidence from (**a**–**g**): (**a**) 1992–1999; (**b**) 1992–2003; (**c**) 1992–2005; (**d**) 1992–2007; (**e**) 1992–2009; (**f**) 1992–2011; (**g**) 1992–2013.

4.2. Permanent GPS Survey

Because this study used GPS data to observe land subsidence, the EW and NS components of GPS were excluded. That is, only vertical components were used to describe the land subsidence. Figure 8 depicts the GPS vertical component, drawn from (a) to (g) according to the location of the GPS stations

from the west to the east of the study area. The negative linear regression slopes of the GPS vertical components indicated that the surface underwent subsidence, and the slopes from the west to the east decreased by −0.0009. Beside the short GPS observation period (Figure 8f), the GPS observation results were consistent with the leveling survey measurements: higher subsidence rate with 6.0 cm/y (Figure 8b–e) in the center of the study area, moderate subsidence rate with 3.1 cm/y (Figure 8a) in the coastal area, and slight subsidence with 0.3 cm/y (Figure 8g) in the western foothills.

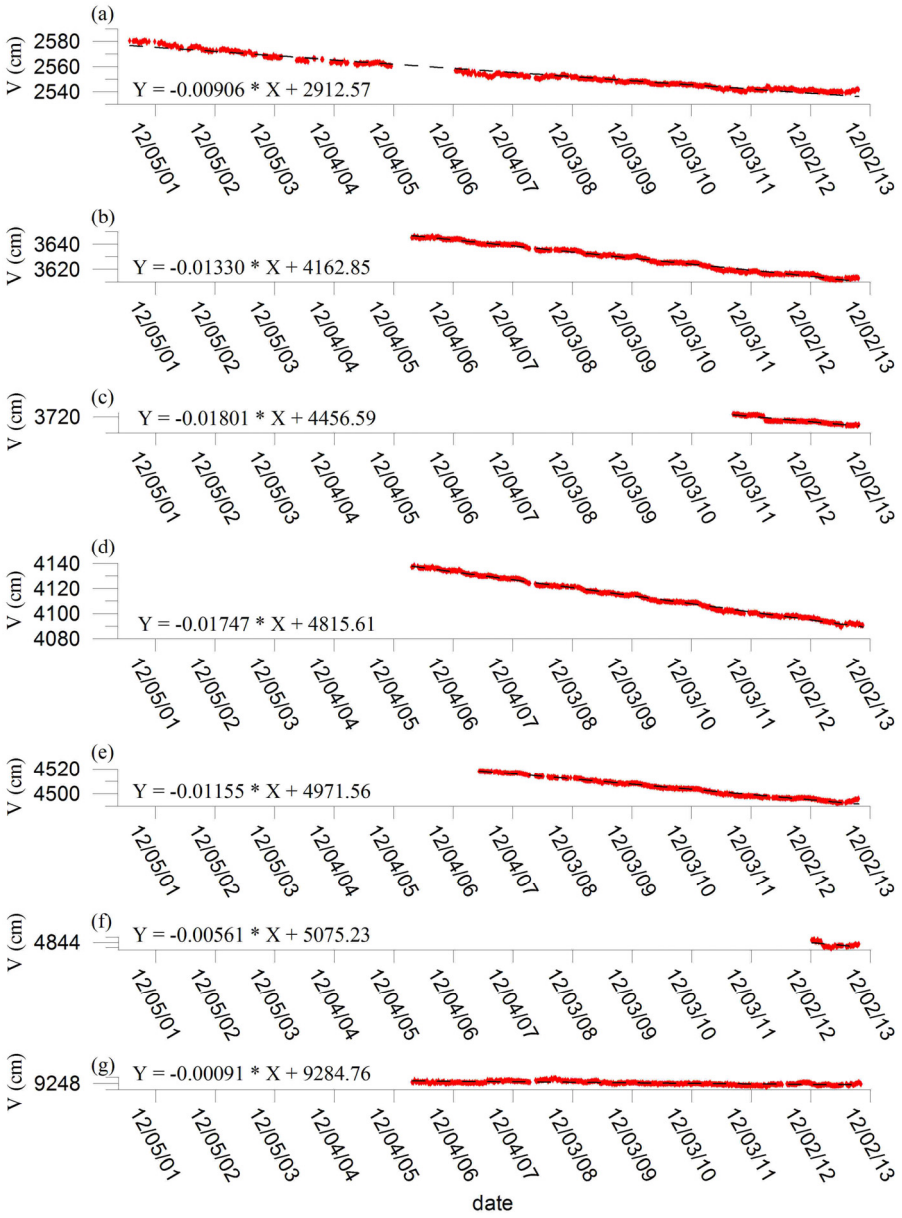

Figure 8. Weekly GPS vertical component draws (**a**–**g**) are ordered from the west to the east of the study area. The dashed line represents the linear-regression fitting line; the slopes from the west to the east decreased.

4.3. Monitoring Wells

Table 3 lists the data recorded by monitoring wells, which are ordered according to their location ranging from west to east. According to the survey span and accumulative subsidence, the subsidence

rate and its mean was calculated. According to the mean subsidence rate, the study area was divided into three parts: severe, moderate, and slight subsidence areas. The subsidence distribution was identical to that identified in the leveling survey. The mean rate in the moderate subsidence area was 1.31 cm/y; the mean rate in the severe subsidence area was 3.04 cm/y; and the mean rate in the slight subsidence area was close to zero.

Table 3. Monitoring wells used in this study (ordered from west to east); the subsidence rate in the center of study area exhibited the maximal scale.

Monitoring Wells No.	Depth (m)	Survey Span	Accumulative Subsidence (cm)	Subsidence Rate (cm/y)	Mean (cm/y)
01	200	1995/07~2013/10	27.60	1.50	
02	200	1995/07~2013/10	28.70	1.60	
03	300	1999/10~2013/10	3.00	0.80	
04	200	1995/11~2013/10	28.40	1.60	
05	300	1996/09~2013/10	49.00	2.90	1.31
06	200	1995/07~2013/10	22.90	1.30	
07	300	1996/08~2013/10	33.90	2.00	
08	300	2008/05~2013/10	3.90	0.70	
10	320	2011/03~2013/10	−2.60	−1.00	
13	300	2008/05~2013/10	9.10	1.70	
09	300	2009/10~2013/10	10.00	2.50	
11	300	2006/04~2013/10	22.40	3.00	
12	300	2003/01~2013/10	59.40	5.50	
14	300	2003/10~2013/10	34.90	3.50	
15	340	2011/03~2013/10	3.40	1.30	
16	300	2007/06~2013/10	19.30	3.00	3.04
17	300	2007/12~2013/10	20.60	3.50	
18	300	2003/12~2013/10	45.00	4.60	
19	300	2007/10~2013/10	13.10	2.20	
20	330	2009/10~2013/10	8.10	2.00	
22	300	2006/04~2013/10	16.90	2.30	
21	300	2008/10~2013/10	1.80	0.40	
23	300	2008/05~2013/10	−1.30	−0.20	0.00
24	300	2007/10~2013/10	−0.90	−0.20	

The monitoring wells were installed at various times. In this study, 17 monitoring wells (Figure 9) that recorded data over 6 years were used to measure the compaction of sedimentary layers. First, the linear regression line was added to the accumulative compaction of the sedimentary layers. The results were divided into linear and exponential types. A trend line of the accumulative compaction of the sedimentary layers exhibiting a linear regression indicates that the compaction of the sedimentary layers is average. The exponential regression, which was located in the northwest and center of the study area, indicated that the compaction phenomenon mainly appeared in deeper sedimentary layers.

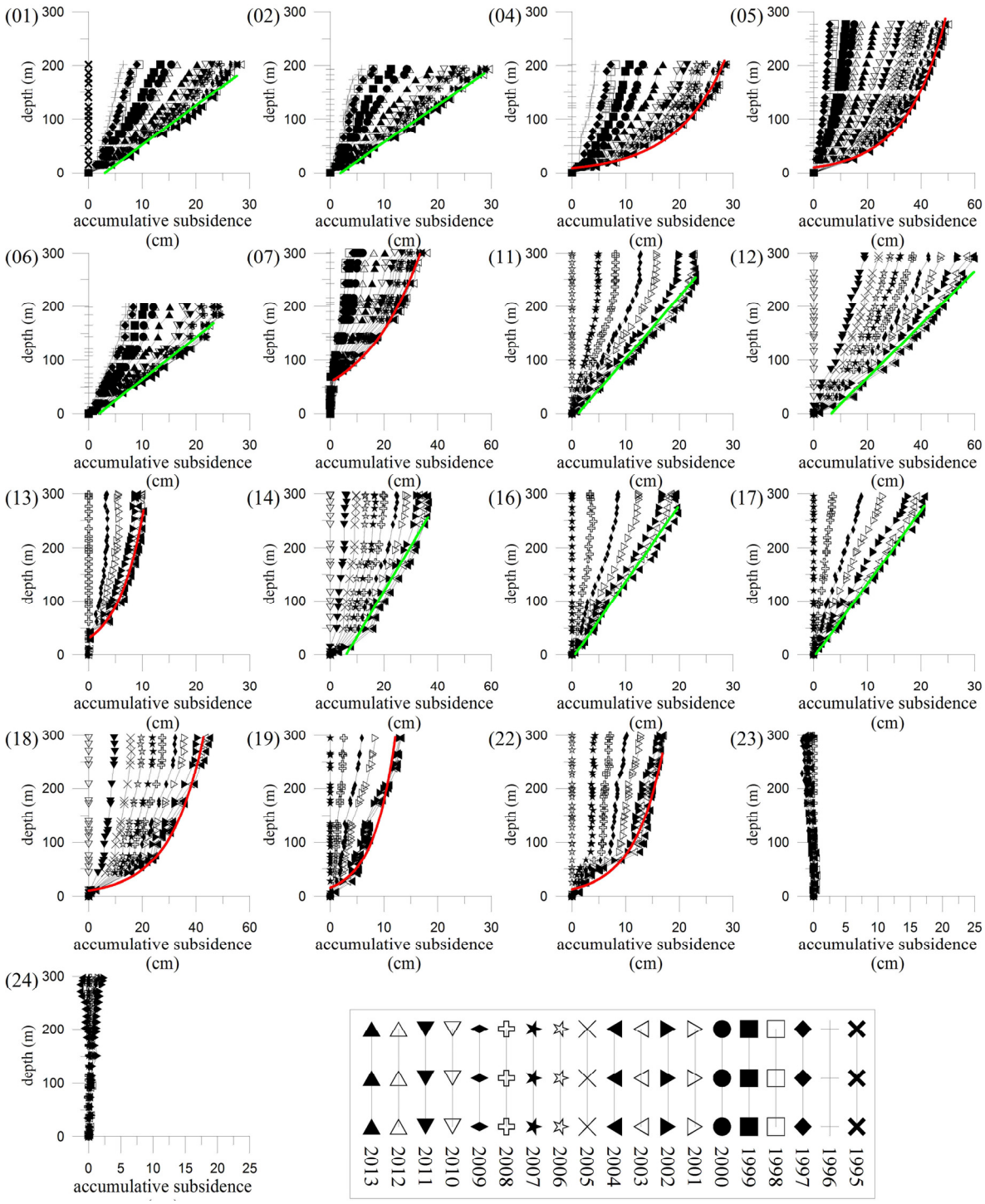

Figure 9. Layer compaction recorded by monitoring wells. The regression line of the total compaction value was calculated. Two types of results were distinguished: linear (green line) and exponential (red line).

4.4. PS-InSAR

Figure 10a shows the results of the vertical deformation of all PS points, and Figure 10b shows a raster map that was interpolated by Kriging method from all of the discrete PS points. The deformation values ranged from −4 cm to +6 cm per year. Comparing the PS-InSAR measurements (Figure 10b) with the leveling survey measurements (Figure 7g) revealed a consistent overall pattern. Beside the coastal area and western foothills the severe and slight subsidence is consistent. The results indicated that the major subsidence areas were in Yuanzhang, Tuku, and Baozhomg township.

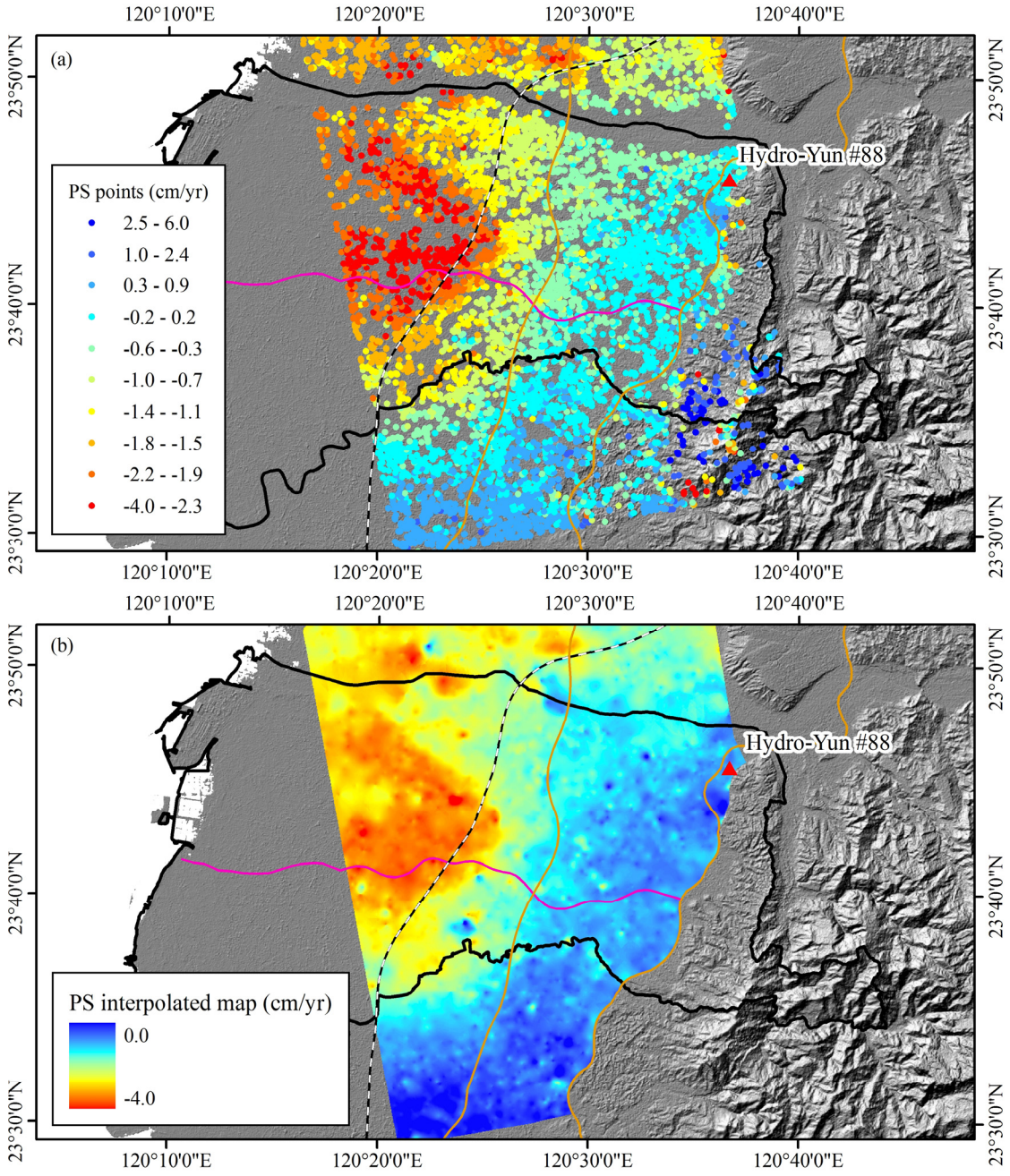

Figure 10. (**a**) SAR mean LOS velocity map from 2007 to 2010; (**b**) raster map interpolated from (**a**).

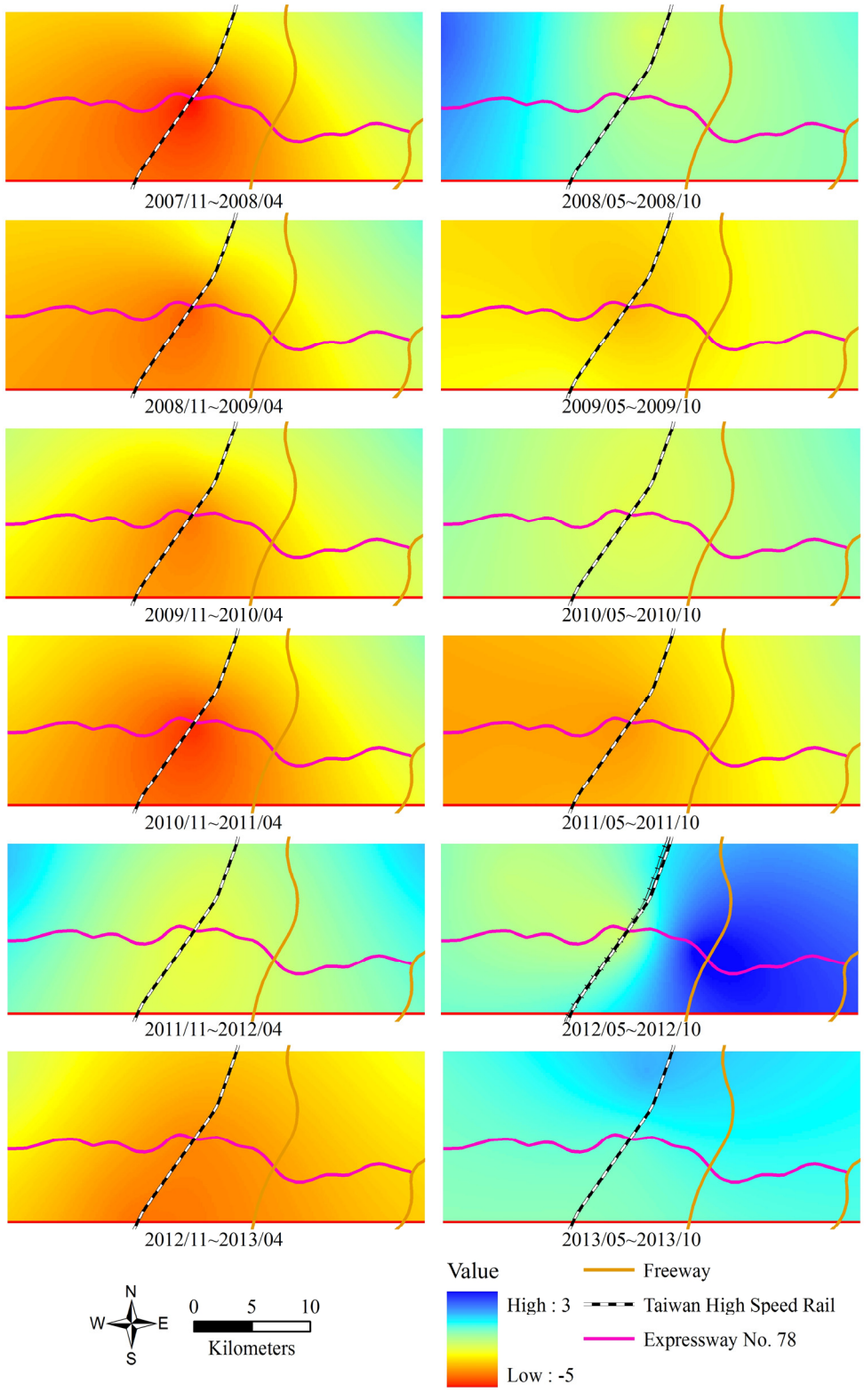

Figure 11. Land subsidence measured using GPS in Yunlin County during dry (**left** images) and wet (**right** images) seasons.

5. Discussion

To understand land subsidence in Yunlin County, GPS data were collected to compare subsidence in the wet and dry seasons. The GPS data were divided into the dry season (November, December, January, February, March, and April) and wet season (May, June, July, August, September, and October) and used the Kriging method to obtain an interpolated map. The vertical uplift movement in the wet season was higher than that in the dry season. However, several vertical uplift movements in the wet season did not exhibit the same level compared with other wet seasons, particularly in 2009, 2010 and 2011 (Figure 11). Subsequently, this study examined the precipitation at Yunlin weather stations from 2007 to 2013 (Figure 12). The precipitation in 2009, 2010 and 2011 was lower than that in the other years. Based on the above analysis, the land subsidence behavior during the wet and dry seasons is partly caused by precipitation. High precipitation in the wet season causes the land subsidence rate to decrease.

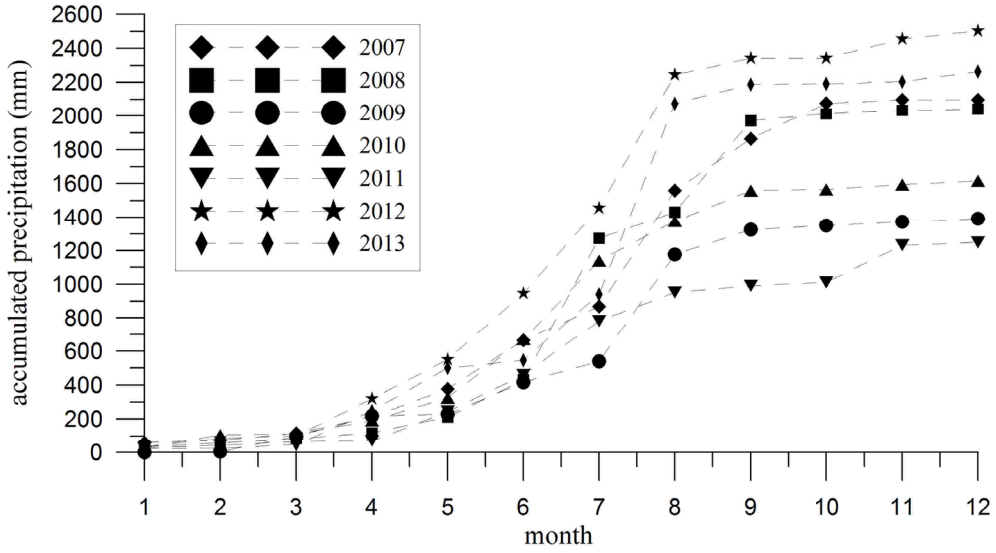

Figure 12. Monthly precipitation in Yunlin County from 2007 and 2013.

This study also used the measurements from the Tuku groundwater well located in the center of the severe subsidence to analyze the relation between water table changes and precipitation. From the 6-year water table changes and precipitation results, it is clear that high precipitation usually accompanies a high water table (Figure 13). The phenomenon indicates effective aquifer recharge is able to mitigate the subsidence, and also produces an interesting question: what is the time lag between water table change and surface subsidence. Therefore, this study utilizes the cross-correlation scheme to examine the time lag between Tuku aquifers 1, 4 water table changes and Tuku GPS vertical movement. The deeper water table changes (aquifer 4) show a less cross-correlation with surface change, but the shallow water table changes (aquifer 1) exhibit a positive cross-correlation (0.415) with surface change by a time lag of around 7 days (Figure 14). These results demonstrate that a rapid surface subsidence or uplift is mainly affected by shallow water table changes.

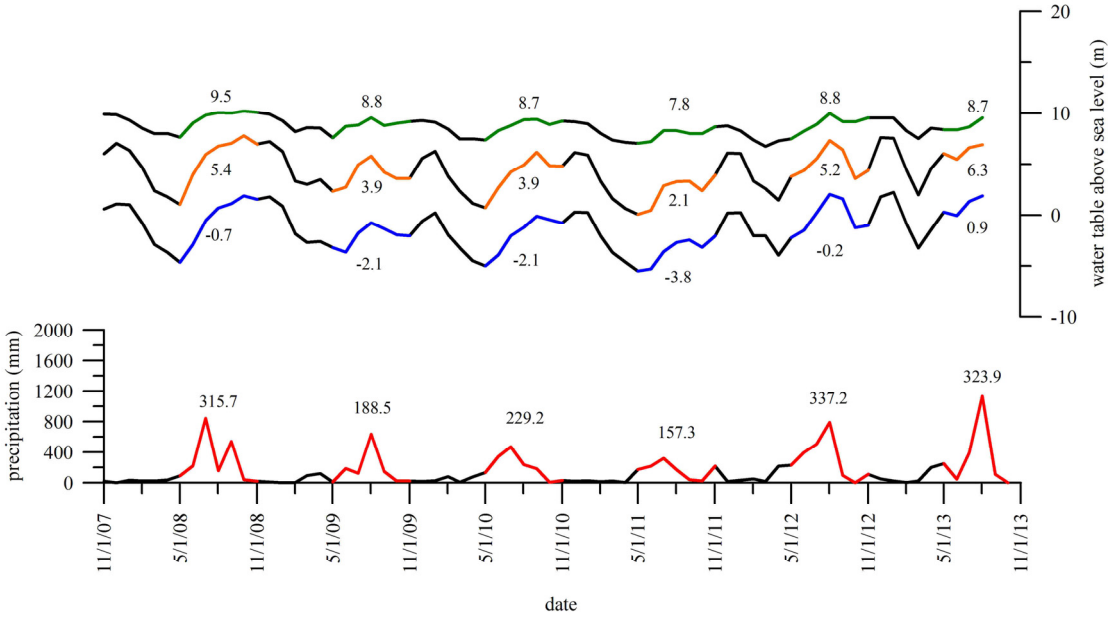

Figure 13. The water table and precipitation data in Tuku well station from 1 November 2007 to 1 November 2013. The lower curve is monthly precipitation and the other 3 curves are water table above sea level in different aquifers (F1, F3, and F4 see Figure 3). In addition, the color curves represent the wet season and the numbers close to the color curves are the mean value.

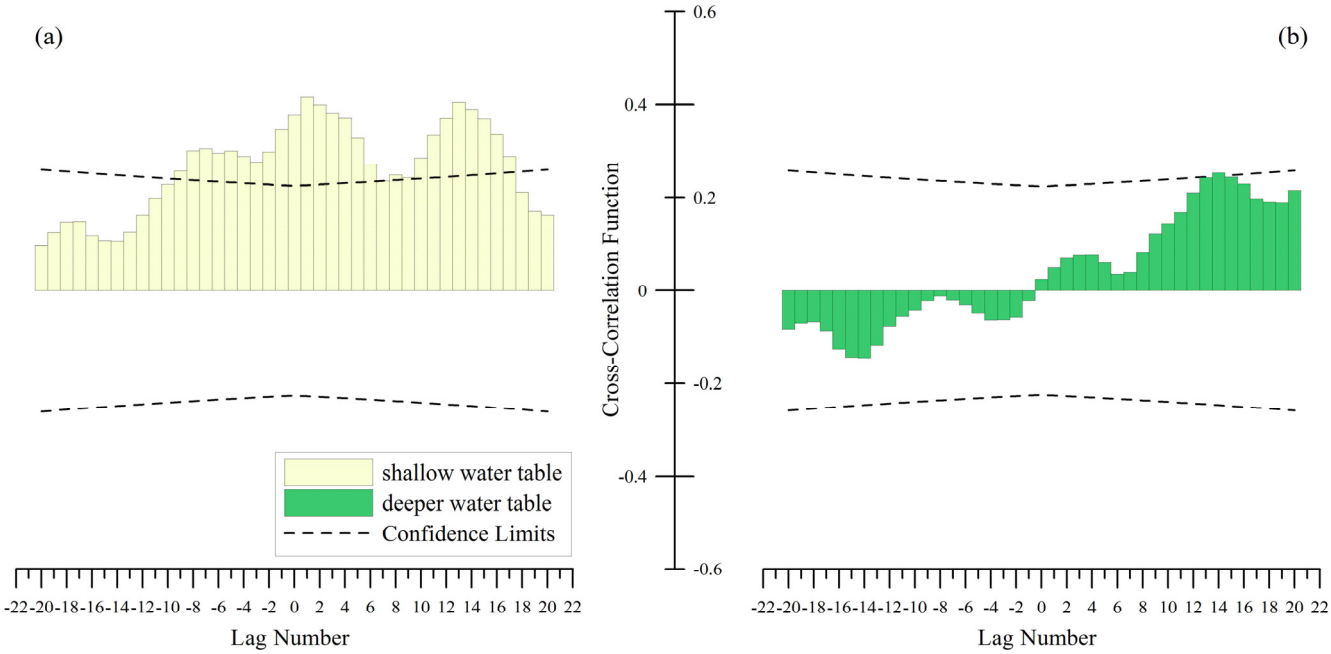

Figure 14. The cross correlation between shallow (**a**) or deeper (**b**) water table changes and Tuku GPS vertical movement. The results show the shallow water table changes and GPS vertical movement have highest coefficient 0.415 in the first week (lag number is 1), indicating that the ground water recharge occurs in the shallow water table and after 7 days vertical movement may be observed. On the other hand, the cross correlation between deeper water table changes and Tuku GPS vertical movement is rather weak.

According to the leveling and GPS survey results, the study area was divided into three subareas: severe subsidence appeared in the center of the study area, moderate subsidence occurred along the coastal area, and slight subsidence existed in the western foothills. According to the long-term survey, the subsidence that occurred in the coastal and central regions of the study area moved toward the east and became severe, a clear boundary demarcated it from the slight subsidence area (dash line in Figure 7). The subsidence rate of the boundary gradually increased over time, whereas the shape of the boundary remained constant, indicating that the boundary reflected the composition of subsurface sediments. According to Central Geological Survey, Ministry of Economic Affairs report [12], the sediments in the study area, from east to west, consisted of gravel, sand, and mud. When groundwater is pumped, the compaction of mud is greater than that of sand and gravel. This study employed a multisensor approach for monitoring land subsidence in Yunlin County. The results showed that land subsidence did not occur uniformly, reflecting the composition of subsurface sediments.

In addition, it is found that the vertical movement of PS-InSAR was consistent with leveling result. By subtracting the interpolated leveling results from PS-InSAR measurements, the effect of horizontal motion, which has an important implication on the behavior of the subsurface aquifer system, can be addressed [20]. However, the horizontal motion is much smaller than the vertical motion in the area of concern. Besides, it has been reported that the vectors of horizontal deformation occur in the same direction with a similar deformation velocity in the study area [19]. This means that the relative horizontal motion approaches zero, while the LOS deformation is converted to vertical deformation, and the effects of horizontal deformation can be ignored. Thus, the horizontal motion is not further discussed in the current work.

The fitting line of the layer compaction value indicates that deep soil compaction occurred in the northwest (Wells 4, 5, 7, and 13) and center (Wells 18, 19, and 22) of the study area. These deep soil compaction areas exhibited a high correlation with severe subsidence, indicating that severe subsidence is caused by deep soil compaction and reflects the composition of subsurface sediments, compaction of subsurface soils, over-pumping of groundwater from deep soils, and deep soil compaction.

According to the groundwater well and land subsidence distributions (Figure 15), the severe subsidence areas did not exhibit any relationship with whole groundwater wells, but a slight correlation with wells deeper than 300 m. According to the leveling, monitoring well, and hydrogeology analysis results, severe subsidence was probably caused by deep groundwater well pumping and reflected the composition of subsurface sediments.

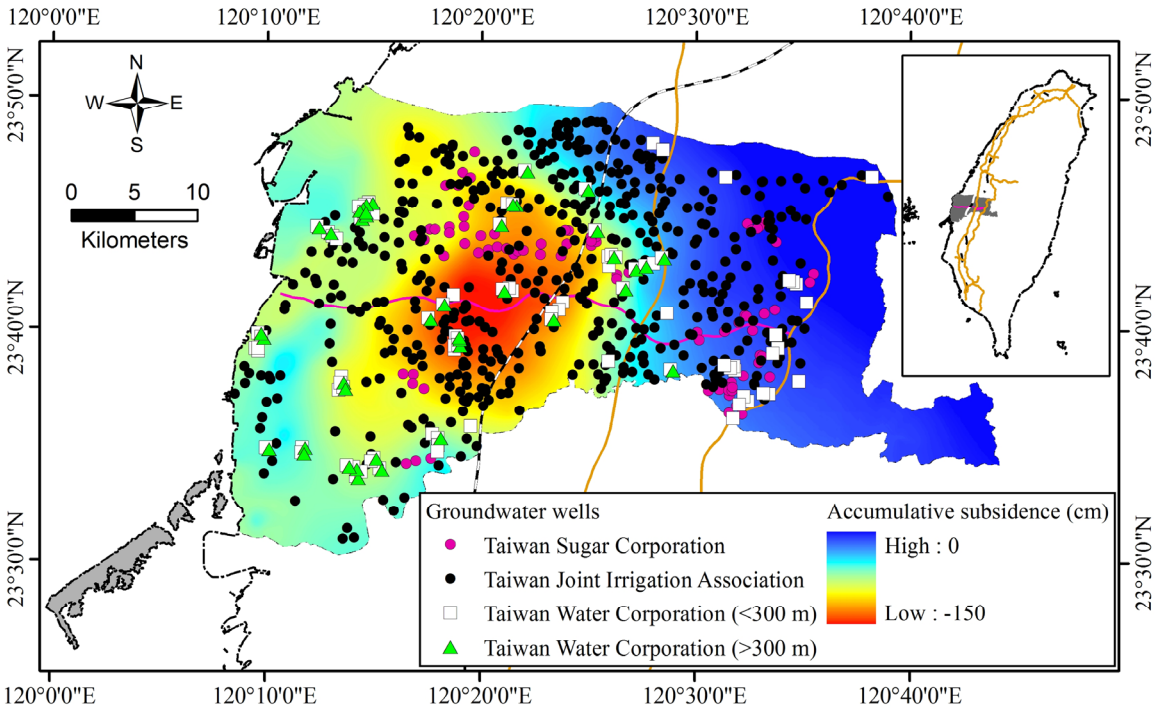

Figure 15. Groundwater well distribution and accumulative subsidence in the study area from 1992 to 2013. The groundwater well locations were adapted from [21].

6. Conclusions

This study involved integrating leveling surveys, continuous GPS stations, monitoring wells, and PS-InSAR to monitor a severe land subsidence area in Yunlin County, Taiwan. The results indicated that a severe subsidence area (7.1 cm/y) was located in the center of the study area, a moderate subsidence area was along the coast (2.3 cm/y), and a slight subsidence area (~0 cm/y) was in the western foothills.

Precipitation substantially affects land subsidence. The shallow water table changes show a high relationship with precipitation, indicating the deeper deep soil compaction is one of the main factors that influence the subsidence.

According to the fitting of the soil compaction values recorded by monitoring wells, groundwater well and land subsidence distributions, this paper proposes that deep soil compaction caused severe land subsidence. The land subsidence is relevant to the composition of subsurface sediments and deep groundwater wells.

Base on the result of a multisensor survey, this study tries to figure out the main factors that influence the distribution of subsidence. Subsidence occurred in west Taiwan, causing many environmental problems and especially affecting the Taiwan High Speed Rail's traffic safety. This study hopes the results will help the government to provide a solution to mitigate the subsidence.

Acknowledgments

Land subsidence has occurred in the Taipei Municipality and Yilan, Changhua, Yunlin, Chiayi, and Pingdong Counties, Taiwan. The Water Resources Agency (WRA), Ministry of Economic Affairs,

began assessing and preventing land subsidence in the 1970s and has mitigated land subsidence in recent years. This study is grateful to the WRA for financial support in completing the survey.

Author Contributions

Wei-Chen Hsu was the principal investigator of the land subsidence projects granted by WRA. En-Kai Lin processed the data and prepared the first short Chinese version of the manuscript draft. Hung-Cheng Chang and Jin-King Liu translated the Chinese draft and re-organized the contents of the manuscript. Hung-Cheng Chang also prepared the drafts of the manuscript revision and responded to the comments. Kuan-Tsung Chang assisted with some parts of the manuscript revision and responding to some of the reviewers' comments on the methodology during the third-round review.

Yuei-An Liou finalized the manuscript and responded to comments from the seven reviewers and three editors by improving the contents and communicating with the editors for all reviews.

Conflicts of Interest

The authors declare no conflict of interest.

References

1. Galloway, D.L.; Jones, D.R.; Ingebritsen S.E. *Land Subsidence in the United States*; U.S. Geological Survey: Reston, VA, USA, 1999; p. 177.
2. Amelung, F.; Galloway, D.L.; Bell, J.W.; Zebker, H.A.; Laczniak, R.J. Sensing the ups and downs of Las Vegas: InSAR reveals structural control of land subsidence and aquifer-system deformation. *Geology* **1999**, *27*, 483–486.
3. Hoffmann, J.; Zebker, H.A.; Galloway, D.L.; Amelung, F. Seasonal subsidence and rebound in Las Vegas Valley, Nevada, observed by synthetic aperture radar interferometry. *Water Resour. Res.* **2001**, *37*, 1551–1566.
4. Motagh, M.; Walter, T.R.; Sharifi, M.A.; Fielding, E.; Schenk, A.; Anderssohn, J.; Zschau, J. Land subsidence in Iran caused by widespread water reservoir overexploitation. *Geophys. Res. Lett.* **2008**, doi:10.1029/2008GL033814.
5. Hasanuddin, Z.A.; Djaja, R.; Darmawan, D.; Hadi, S.; Akbar, A.; Rajiyowiryono, H.; Sudibyo, Y.; Meilano, I.; Kasuma, M.A.; Jahar, J.; Subarya, C. Land Subsidence of Jakarta (Indonesia) and its Geodetic Monitoring System. *Nat. Hazards* **2001**, *23*, 365–387.
6. Hung, W.C.; Hwang, C.; Chang, C.P.; Yen, J.Y.; Liu, C.H.; Yang, W.H. Monitoring severe aquifer-system compaction and land subsidence in Taiwan using multiple sensors: Yunlin, the southern Choushui River Alluvial Fan. *Environ. Earth Sci.* **2010**, *59*, 1535–1548.
7. Hung, W.C.; Hwang, C.; Chen, Y.A.; Chang, C.P.; Yen, J.Y.; Hooper, A.; Yang, C.Y. Surface deformation from persistent scatterers SAR interferometry and fusion with leveling data: A case study over the Choushui River Alluvial Fan, Taiwan. *Remote Sens. Environ.* **2011**, *115*, 957–967.
8. Hsu, W.C.; Liu, J.K.; Liou, Y.A.; Wu, M.C.; Hwang, J. T.; Hsieh, C.S.; Tsai, C.R.; Zakharov, A.I. *Multi-Sensor Observations of Land Subsidence in Taipei, Changhua, and Yunlin Areas*; Water Resources Agency, Ministry of Economic Affairs Taiwan: Taipei, Taiwan, R.O.C., 2011; p. 308.

9. Hsu, W.C.; Liu, J.K.; Lin, T. Y.; Liou, Y.A.; Wu, M.C.; Hwang, J. T.; Tsai, C.R.; Wu, J.H. *Multi-Sensor Observations of Land Subsidence in Taipei, Changhua, and Yunlin Areas*; Water Resources Agency, Ministry of Economic Affairs Taiwan: Taipei, Taiwan, R.O.C., 2012; p. 285.
10. Hou, C.S.; Hu, J.C.; Shen, L.C.; Wang, J.S.; Chen, C.L.; Lai, T.C.; Huang, C.; Yang, Y.R.; Chen, R.F.; Chen, Y.G.; *et al.* Estimation of subsidence using GPS measurements, and related hazard: The Pingtung Plain, southwestern Taiwan. *Comptes Rendu Geosci.* **2005**, *337*, 1184–1193.
11. Tung, H.; Hu, J.C. Assessments of serious anthropogenic land subsidence in Yunlin County of central Taiwan from 1996 to 1999 by Persistent Scatterers InSAR. *Tectonophysics* **2012**, *578*, 126–135.
12. Chiang, C.J.; Lai, T.C.; Lai, T.H.; Huang, C.C.; Fei, L.Y.; Hou, C.S.; Chen, J.E.; Chen, L.C.; Lu, S.Y.; Chou, S.C. *Hydrogeological Survey Report of Chosui River Watershed*; Central Geological Survey: Taipei, Taiwan, 1999; p. 129.
13. Beutler, G.; Bock, H.; Dach, R.; Fridez, P.; Gade, A.; Hugentobler, U.; Jaggi, A.; Meindl, M.; Mervart, L.; Prange, L.; *et al*. *Bernese GPS Software*; Dach, R., Hugentobler, U., Fridez, P., Meindl, M., Eds.; Astronomical Institute University of Bern: Bern, Switzerland, 2007.
14. Wang, C.S.; Liou, Y.A. A study on the relationship between seasonal tropospheric variation and positioning accuracy by GPS. *J. Photogramm. Remote Sens.* **2006**, *11*, 191–200.
15. Wang, C.; Liou, Y.A.; Yeh, T. Impact of surface meteorological measurements on GPS height determination. *Geophys. Res. Lett.* **2008**, *35*, L23809.
16. Mora, O.; Mallorqui, J.J.; Broquetas, A. Linear and nonlinear terrain deformation maps from a reduced set of interferometric SAR images. *IEEE Trans. Geosci. Remote Sens.* **2003**, *41*, 2243–2253.
17. Yang, C.H.; Tsay, J.R.; Su, P.T. Improved PS-InSAR Algorithm for Determining Subsidence in Central Taiwan. *J. Photogramm Remote Sens*. **2015**, *19*, 171–187.
18. Yang, J.S. An improved PS-InSAR Approach. Master's Thesis, Department of Geomatics, National Cheng Kung University, Tainan, Taiwan, 2011.
19. Hung, C.J. Establishing a Horizontal Velocity Model of Taiwan Using GPS Observations and the Least-squares Collocation Technique. Master's Thesis, Department of Geomatics, National Cheng Kung University, Tainan, Taiwan, 2012.
20. Hoffmann, J.; Zebker, H.A. Prospecting for horizontal surface displacements in Antelope Valley, California, using satellite radar interferometry. *J. Geophys. Res.: Earth Surface* **2003**, *108*, 6011, doi:10.1029/2003JF000055.
21. Kung, C.S. *Conjunctive Use of Surface and Groundwater in Cho-Shui Creek Fan Study and Evaluation on Water Utilization Measures*, Water Resources Agency, Ministry of Economic Affairs Taiwan: Taichung office, Taiwan, R.O.C., 2007.